Molecular Dynamics Simulation Study of Molecular Ejection Mechanisms: keV Particle Bombardment of C_6H_6/Ag{111}

Reema Chatterjee, Zbigniew Postawa,[1] Nicholas Winograd, and Barbara J. Garrison*

Department of Chemistry, The Pennsylvania State University, University Park, Pennsylvania 16802

Received: August 6, 1998; In Final Form: October 21, 1998

Molecular dynamics simulations have been performed to gain microscopic insight into the factors that lead to molecular ejection after ion bombardment of an organic overlayer on a metal surface. The specific system modeled is benzene (C_6H_6) adsorbed on Ag{111}. The kinetic energy and angular distributions of C_6H_6 molecules obtained from the simulations match well with the experimentally measured distributions. The angular distributions of C_6H_6 molecules show both normal and off-normal components. Analysis of individual trajectories reveal that the off-normal ejection arises from single collisions between substrate Ag atoms and C_6H_6 molecules, while multiple collisions result in low-energy ejection along the surface normal. To separate issues of rotational and vibrational excitation from translational motion, calculations are also performed on an atomic adsorbate with a mass similar to that of C_6H_6.

Introduction

There is a continuing interest in elucidating the mechanisms of molecular desorption from surfaces bombarded by energetic (keV) ion beams. The experiments are finding wide application in areas as diverse as imaging of biological samples, processing of electronic materials, and characterization of polymers.[2] Progress toward obtaining a general theory of desorption has been difficult, however, partly from a lack of a molecular-level vision of the energy dissipation process in the molecular layer. Recent experiments aimed toward measuring the trajectories of desorbed neutral molecules from bombarded molecular films have been designed to acquire this vision.[3] So far, the results are quite complicated since they show that, depending upon the nature of the system, various mechanisms may dominate the desorption event.[4] These mechanisms include desorption induced by collision cascades within a metallic substrate,[3,5–8] thermal desorption initiated by ion-beam-induced reactions,[9–11] desorption stimulated by electronic de-excitation,[12–14] and thermal-like desorption arising from collision cascades formed within a molecular film.[3]

Although these experiments are helpful, a molecular-level understanding of the energy dissipation process can also be obtained using molecular dynamics (MD) computer simulations. These calculations have been used successfully for many years to explain the sputtering of atomic solids.[15–18] The strategy involves integrating the classical equations of motion in order to obtain the trajectories of atoms and molecules that leave a solid due to bombardment by energetic particles. The calculated quantities, such as energy and angle distributions, are then compared with experimentally obtained trajectories. If there is agreement, the atomic-level mechanisms can be extracted from the dynamics to better understand the process. This synergism between theory and experiment is particularly powerful and has allowed us over the years to obtain near-quantitative agreement between measured and calculated distributions for atomic solids.[18,19,20]

On the other hand there have been only a few attempts to perform MD calculations on molecular systems. The unavailability of a many-body interaction potential for hydrocarbon systems is the primary reason for the lack of progress. One of the first MD studies utilized pairwise interaction potentials to examine how a molecule such as benzene with chemical bond strengths of ~4–6 eV adsorbed on a metal substrate could be ejected intact by a projectile with several thousand electronvolts of kinetic energy.[21–23] This qualitative model clearly showed that more than one substrate atom with energy in the 10–50 eV kinetic energy range could simultaneously collide with the benzene molecules to induce desorption without breaking bonds. Recently, improved potential functions have become available[24,25] and simulations of overlayers of ethylidyne type species have been performed.[26–30] Reactions such as H atom abstraction by a fragment of an adjacent molecule, preferential shearing off of the top of adsorbed chains, and unimolecular rearrangement have been predicted. In addition, there have been simulations aimed toward understanding ejection of alkane thiols on a metal surface[31] and polyatomic projectile bombardment of organic overlayers.[32] At the present level of sophistication, it appears that the modeling is capable of quantitatively predicting a number of experimental parameters.

There is now a limited set of experimental data on organic overlayers that are amenable to be directly modeled using the MD approach.[3] These experiments were performed on sub-monolayer amounts of C_6H_6 molecules adsorbed on Ag{111} by bombardment with 8 keV Ar^+ ions followed by measurement of the trajectories of the desorbed neutral C_6H_6 molecules. The results show that when very few C_6H_6 molecules are present on the surface, the energy and angular distributions of the molecules reflect the corresponding distributions of the ejecting metal substrate atoms. For example, the distributions exhibit a peak kinetic energy of 1.25 eV and exhibit polar angular anisotropy characteristic of the substrate crystal. At slightly higher coverages, however, the peak in the kinetic energy distribution shifts to lower values, and the angular distribution loses much of its structure.

Here we use MD simulations to help elucidate the mecha-

---

152 *J. Phys. Chem. B, Vol. 103, No. 1, 1999*

Chatterjee et al.

nisms of ejection of molecular films due to particle bombardment. The check on the reliability of the calculations is quantitative comparisons to experimental energy and angle distributions from the C_6H_6/Ag{111} system. By using many-body potentials for the Ag substrate, a reactive hydrocarbon potential for the C_6H_6 overlayer and a Lennard–Jones potential between the two, we are able to reproduce the essence of the experimental energy and angular distributions for submonolayer coverages of benzene. The results of the calculations are then used to probe the mechanistic details of the critical atomic motion that is responsible for ejecting the molecules. Moreover, to separate issues of rotational and vibrational excitation from translational motion, calculations are performed for an atomic adsorbate with a mass similar to that of C_6H_6. Finally, we propose new spectroscopic experiments aimed at confirming the degree of internal excitation in C_6H_6 and at correlating this energy with observed translational energy and angular distributions.

Methodology

The molecular dynamics scheme used in this work is described in extensive detail elsewhere.[15,33,34] Briefly, it consists of integrating Hamilton's equations of motion over some time interval to predict the resulting position and velocity of each atom in the system. The energy and forces in the system are described by many-body potential-energy functions. The quality of the potential energy surface is important as it governs the reliability of the results from the simulation. Experimentally observable properties, such as total yield, mass spectrum, kinetic energy and angular distributions, can be calculated from the final positions, velocities, and masses of all the ejected species. Mechanistic information can be obtained by monitoring the time evolution of important collisional events.

The model approximating the Ag{111} substrate consists of a finite microcrystallite containing 1404 Ag atoms arranged in nine layers of 156 atoms each. Fourteen C_6H_6 molecules are placed parallel to the crystal surface above the hcp 3-fold sites (i.e., above a second-layer atom) in a (3×3) configuration as shown in Figure 1. This configuration was chosen because benzene adsorbed on a Ag{111} surface at low temperatures is known to lie flat in an ordered (3×3) overlayer.[35] The crystal size was chosen to minimize edge effects on the dynamical events leading to ejection of molecules. The polar (θ) and azimuthal (ϕ) angles have been defined in the inset to Figure 1.

The forces among the atoms are described by the best currently available empirical potential energy functions that describe the system of interest. The Ag–Ag interactions are described by the molecular dynamics/Monte Carlo corrected effective medium (MD/MC–CEM) potential for fcc metals.[36–38] The MD/MC-CEM potential has been used in the past to calculate the energy and angular distributions of ion-bombarded Rh and Ni.[18] The Ar–Ag, Ar–C, and Ar–H interactions are described using the purely repulsive Molière pairwise additive potential.[39]

The Brenner potential for hydrocarbons is used to describe the C–C, C–H, and H–H interactions.[24,25] This potential allows for chemical reactions and accompanying changes in atomic hybridization and has been used for a number of different reaction conditions[40] including energetic particle bombardment.[26–32] The Brenner potential can describe chemical reactions, however, it does not include the long-ranged van der Waals type interactions. Hence, collisions between molecules in which the molecules merely alter each other's motion cannot be described. It is because of this condition of the potential that

we restrict our comparisons to experimental data for a system of very low coverage of C_6H_6 molecules on Ag{111} where the molecules are too far apart to interact with each other. As described previously, a Molière function is attached to the repulsive wall of the Brenner hydrocarbon potential to handle energetic collisions.[26]

The final interactions that need to be described are those between the Ag substrate and the C and H atoms. Previously we have described potentials for two types of interactions— one in which there are strong chemical bonds between the organic molecule (e.g., ethylidyne) and the substrate,[26] and one in which there are weaker interactions of the organic molecule (e.g., biphenyl) and the substrate.[32] Since the Ag–C_6H_6 interactions are initially π-like in character, we choose to describe them by Lennard–Jones potential functions which are pairwise additive for both the Ag–C and Ag–H interactions. The Lennard–Jones parameters are chosen such that the binding energy of the molecule C_6H_6 to the Ag{111} surface is 0.4 eV.[41] The Ag–C and Ag–H distances of 2.3 Å are taken from an estimate for the height of C_6H_6 above the Ag{111} surface.[35,42] All the parameters for the Lennard–Jones potential are given in Table 1. For computational efficiency the mass of hydrogen is taken be that of tritium ($m = 3$). The mass of the molecule is therefore 90 amu instead of 78 amu. All the plots and discussion, however, are reported as if the hydrogen mass ($m = 1$) is used in order to reduce confusion when making comparisons to experimental spectra.

The projectile impinges normal to the surface with an initial kinetic energy of 500 eV. To reproduce the experimental conditions, the primary ion must sample the entire surface or a symmetrical equivalent in the case of an ordered surface. The appropriate impact zone for an ordered (3×3) C_6H_6 film on Ag{111} is shown in Figure 1. A total of 1000 trajectories are calculated and the impact points cover the impact zone in a systematic fashion. Each trajectory is initiated with a fresh sample with all the atoms in their equilibrium positions. The trajectory is terminated when the total energy of all the atoms remaining in the solid is not sufficient for any further ejection. This time ranges between 0.5 and 1.8 ps and depends on the impact point of the primary particle and the manner in which the energy distributes within the solid. Open boundary conditions are used so that the particles are allowed to leave the sides and bottom of the crystallite.[33]

Finally, MD simulation studies are performed for an atomic adsorbate to disentangle the ejection mechanisms of adsorbates from the complications of internal motions including dissociation associated with the benzene molecule. These calculations were done for an atomic adsorbate whose mass is closest to that of our C_6H_6 molecule. The element of choice is zirconium with mass close to 91 amu. The Zr–Ag interactions are also described by a Lennard–Jones potential function. The parameters are chosen such that the atom has the same binding energy to the surface of 0.4 eV as the C_6H_6 molecule. The Zr–Zr interactions are described by a purely repulsive Molière pairwise potential as we are trying to test the effect of long-range repulsions of the molecular overlayers on the ejection events. The calculations are performed with the Zr atoms placed in the same site as the C_6H_6 molecule, i.e., hcp 3-fold site, in (3×3) and (1×1) coverages.

Results and Discussion

In this study we present the results of MD simulations of keV particle bombardment of C_6H_6/Ag{111} and compare them to experimental measurements. The kinetic energy distributions are discussed first because they give an idea of the energetics
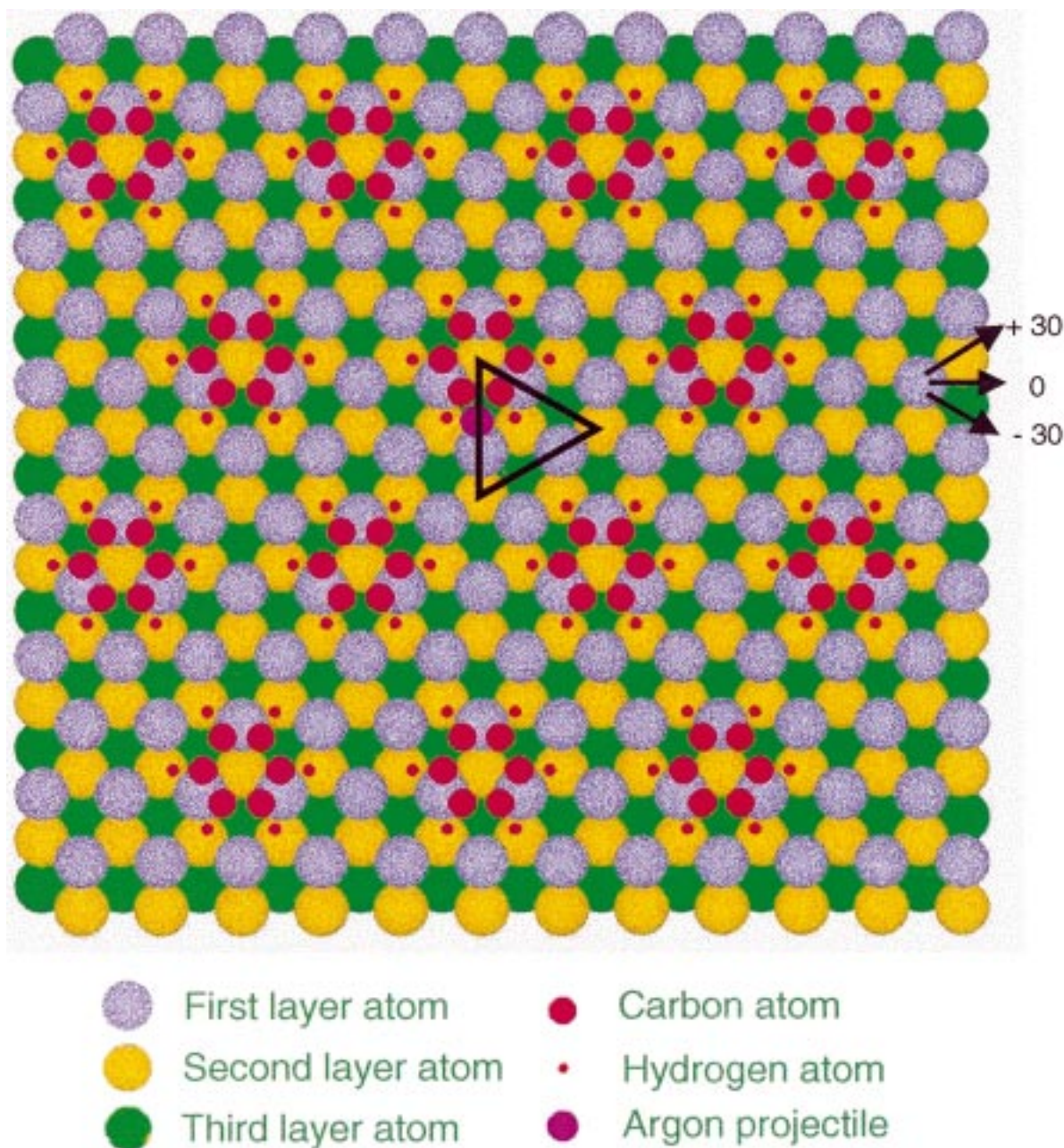
Figure 1. The film configuration of a (3 × 3) ordered overlayer of C$_6$H$_6$ on Ag{111}. The impact zone is represented by the triangle. The arrows indicate the three azimuthal directions. The coloring scheme is shown on the figure.

TABLE 1: The Ag−C and Ag−H Lennard−Jones 6/12 Parameters[a]

	σ (Å)	ϵ (eV)
Ag−C	2.3	0.031
Ag−H	2.3	0.005
Ag−Zr	2.3	0.105

[a] The σ parameter is defined as per ref 26 and is the equilibrium separation.

of the collision process and are most easily interpreted. Next, we examine the reasons behind an experimentally observed shift in the peak kinetic energy of C$_6$H$_6$ with coverage by using an atomic adsorbate to disentangle the influence of rotational and vibrational excitation. And finally, we show that the calculated angular distributions of ejected C$_6$H$_6$ molecules are consistent with the experimental data. These angular distributions are then used to identify the important mechanisms that lead to molecular ejection.

The temporal evolution of a typical collision event leading to ejection of atoms and molecules from the crystal into the vacuum is shown in Figure 2. The equilibrium configuration of the solid and the position of the projectile before impact is shown in the top snapshot of atomic positions. In this example after 500 fs, Ag, Ag$_2$, C$_6$H$_6$, and C$_2$H$_2$ species already appear above the surface as is shown in the bottom snapshot. By averaging over all 1000 trajectories a calculated mass spectrum is obtained as is shown in Figure 3. Calculated mass distributions are determined by counting the neutral clusters that exist 1−2 ps after the bombardment event and are not adjusted for ionization probabilities, ion stabilities, or possible fragmentation of the clusters during their μs flight to the detector. The mass spectrum exhibits peaks for Ag, Ag$_2$, C$_6$H$_6$, C$_2$H$_2$, C$_2$H, C$_6$H$_5$, CH, C, H, AgC$_6$H$_6$, and Ag$_2$C$_6$H$_6$ along with other less pronounced species. Since the primary aim of this study is to understand molecular ejection as it relates to energy and angular distributions of parent molecules, we will focus on the ejection
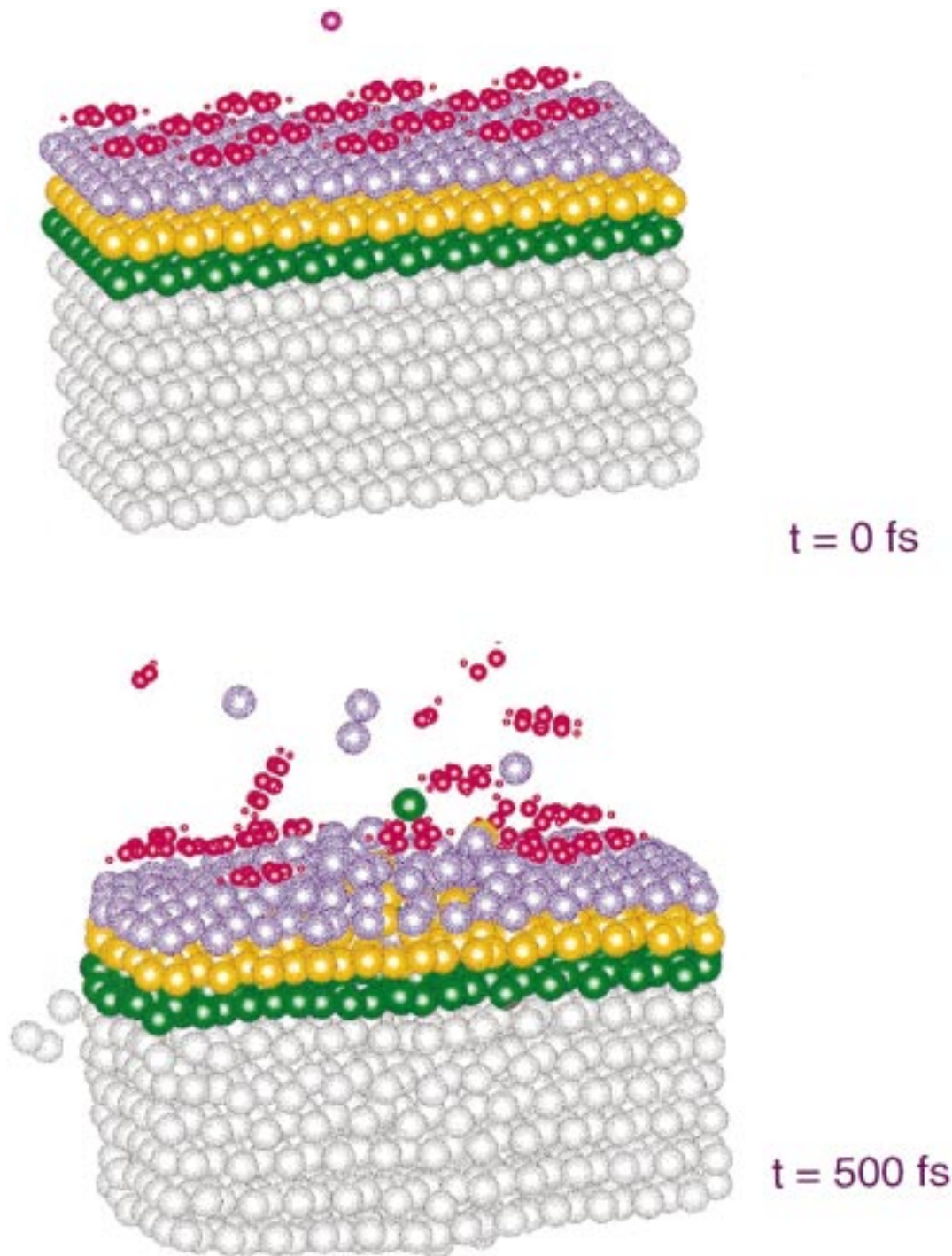
Figure 2. Example of a trajectory calculated for 500 eV Ar bombardment of $C_6H_6/Ag\{111\}$. Frame 1 is prior to the Ar atom bombardment ($t = 0$). Frame 2 depicts the system 500 fs after the primary ion impact. The coloring scheme is the same as in Figure 1.

of C_6H_6 molecules. Another investigation is addressing the issue of the complete mass spectrum of ejected alkanethiol molecules.[43]
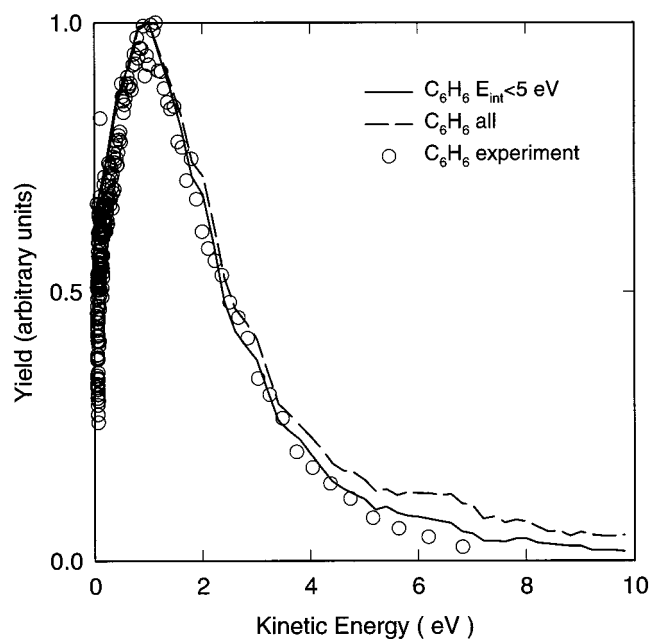
Kinetic Energy Distributions

The calculated kinetic energy distribution of C_6H_6 is plotted along with the experimental distribution for 0.2-monolayer (ML) coverage in Figure 4. As mentioned earlier, the hydrocarbon potential does not incorporate the long-range intermolecular interactions necessary to describe collisions between benzene molecules. Therefore, it is important to compare the calculations with experimental results obtained at very low coverage where the interaction between C_6H_6 molecules is minimal. Our earlier

studies have shown that below 0.2 ML coverage the C_6H_6 molecules are too far apart to interact with each other.[3] Therefore, while the experimental distributions measured at or below 0.2 ML C_6H_6 coverage can be compared with the calculated results, comparison of high-coverage data is beyond the scope of this work. As is clear from the figure, the calculated kinetic energy distribution (dashed line) matches well with the experimental distribution (open circles), although there is some discrepancy for energies greater than 4 eV.

The C_6H_6 molecules which are counted for Figures 3 and 4 are those which exist 1−2 ps after the bombardment event, i.e., at the termination of a trajectory. It is possible that molecules with high internal energies will fragment during the microsecond
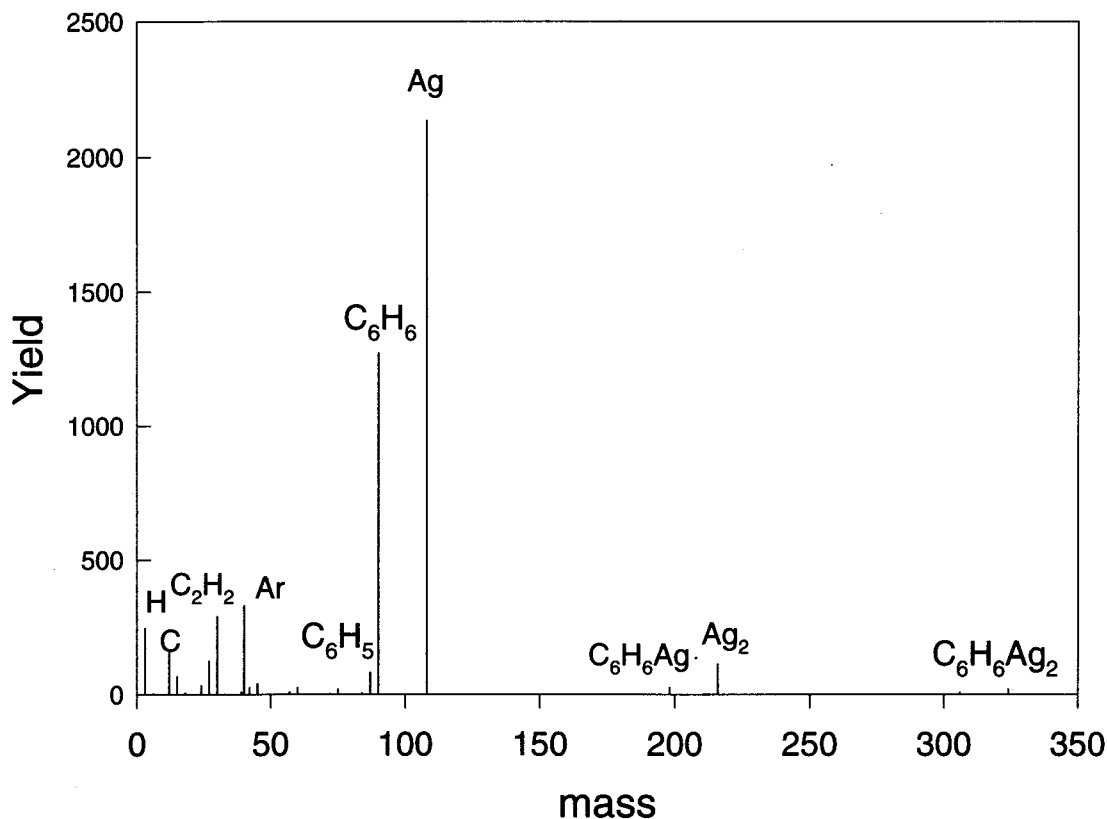
Figure 3. The calculated mass spectrum of all the species ejected after 500 eV Ar atom bombardment of $C_6H_6/Ag\{111\}$. As explained in the text, the tritium isotope of hydrogen is used in the calculation, but the masses in the spectrum use the mass of H.

Figure 4. The calculated kinetic energy distributions, (broken lines) for all the ejected C_6H_6 molecules and (solid lines) for all C_6H_6 molecules with total internal energies less than 5 eV. The circles depict the experimental kinetic energy distribution of neutral C_6H_6 molecules for 0.2 ML coverage.[3]

flight time to the detector.[44] To assess the importance of fragmentation we calculate the internal energy of the C_6H_6 molecules. As shown previously[26] the total internal energy, E_{int}, of each group of atoms comprising one C_6H_6 molecule is calculated as follows:

$$E_{int} = V(r_{ij}) + ke(r_{ij}) - V_{eq}$$
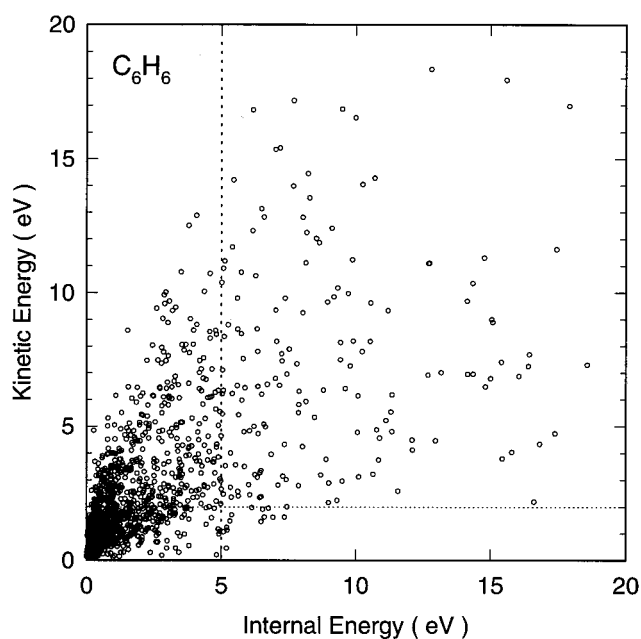
Figure 5. The scatter plot correlating the kinetic energies of the ejected C_6H_6 molecules with their internal energies.

where $V(r_{ij})$ and $ke(r_{ij})$ are the potential and kinetic energies of the atoms relative to the center of mass calculated from the atomic coordinates and velocities at the termination of the collision cascade and V_{eq} is the equilibrium potential energy of the molecule. The scatter plot correlating the kinetic energies of the molecules with their internal energies is presented in Figure 5. There is a clear correlation between the internal energy and kinetic energy of ejected molecules. The molecules with higher internal energies tend to have higher kinetic energies.

The issues are how many of the molecules will dissociate and not be detected and how does this influence the experimentally observed properties such as energy distributions. We could go through an analysis as done previously for small metal clusters[44] and continue integrating the equations of motion for the C_6H_6 molecules to longer times to see if they will fragment. In this case, however, we do not believe that the empirical potential is sufficiently good for all the possible reaction channels such that this exercise is warranted. Thus we make a simple estimate of a 5 eV cutoff for dissociation as denoted by the vertical dashed line in Figure 5. This value is probably slightly larger than the lowest fragmentation channel but is a compromise choice so as not to throw too many particles from the analysis of the results for the simulation. With this definition we predict that ∼89% of the benzene molecules will be detected.

The energy distribution plot can now be adjusted for dissociation of molecules. As shown by the solid line in Figure 4, the agreement between the calculated and measured energy distributions markedly improves, especially in the high-energy regime. The low-energy portion of the energy distribution plot is virtually unchanged by correcting for molecules that dissociate. As shown by the horizontal dashed line at 2 eV in Figure 5, almost all the molecules with low kinetic energies also have low internal energies. Based on the above analysis, only molecules with internal energies less than 5 eV will be used in the subsequent analyses.

The energy transfer from the primary ion into a molecular system is a combination of excitation of the translational and internal modes of the molecules. The information contained in the kinetic energy distributions is therefore a convolution of the two processes. To better understand the molecular ejection mechanisms it is important to be able to separate the collisional processes that lead to the ejection of the adsorbate from those such as internal excitation that are unique to adsorbed molecules. To address these issues, we performed MD simulations in which the C_6H_6 molecule is replaced with an atomic adsorbate that has a similar mass and is bound to the surface by the same binding energy. Since coverage-dependent calculations cannot be performed for C_6H_6, this simpler atomic system is also used to investigate how the adsorbate coverage influences the distributions. It should be noted that the C_6H_6 molecule is bigger in size than the atom so, even though they are both placed in the same site on the crystal surface, the C atoms in the C_6H_6 molecules lie right above the three first-layer Ag atoms, while the atomic adsorbate, being smaller, lies in the center right above a second-layer Ag atom. This difference does influence the distributions. We are therefore using the atomic adsorbate as a model to compare and explain observed trends but not to compare absolute values.

The kinetic energy distributions for the atomic adsorbate are shown in Figure 6 for both the (3×3) and (1×1) ordered overlayers. The kinetic energy distributions are clearly influenced by the adsorbate coverage. As the coverage increases, the peak in the energy distribution shifts to a lower value. The atoms ejecting from the (3×3) overlayer have a peak energy close to 0.8 eV, while those ejecting from the (1×1) surface eject with a peak energy close to 0.5 eV. This shift in the kinetic energy distribution at higher coverage is also observed experimentally for C_6H_6 as shown in the inset to Figure 6. The experimental kinetic energy distributions of C_6H_6 molecules for 0.2 and 1 ML coverage of C_6H_6/Ag{111} are shown in the inset in Figure 6. In both the experimental and the calculated distributions, an increase in adsorbate coverage shifts the peak in the energy distribution to lower values. This shift to lower
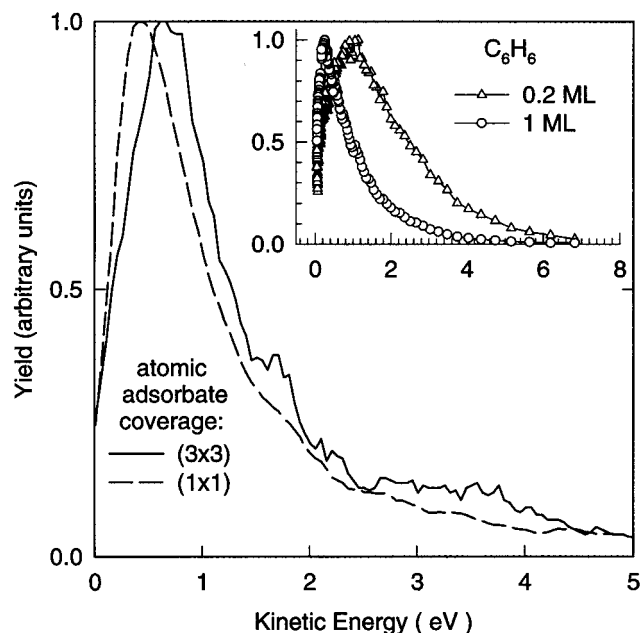

Figure 6. The calculated kinetic energy distributions of the atomic adsorbate for two different coverages on Ag{111}. The inset shows the experimental kinetic energy distributions[3] of neutral C_6H_6 molecules ejected after 8 keV Ar^+ ion bombardment of C_6H_6 adsorbed on Ag-{111} at 0.2 ML coverage (Δ) and 1 ML coverage (○).

peak energies as the coverage increases is due to an enhanced number of collisions between adsorbate species, which reduces their peak kinetic energies.

The one theory that relates the peak position in the energy distribution to properties of the system is due to Thompson and was developed for bulk amorphous atomic systems.[45] The Thompson model predicts that the peak position in the kinetic energy distribution of atoms sputtered from amorphous solids should be equal to half the binding energy. For metal systems this observation is approximately true although there is a tendency for the peak position to be slightly higher than predicted. In any case, the peak position is certainly less than the surface binding energy.[16] For the adsorbate cases, however, the peak in calculated kinetic energy distributions of C_6H_6 (∼1 eV) and the atomic adsorbate (∼ 0.8 eV) are more than twice the binding energy (∼0.4 eV). It is not surprising that the energy distributions of the adsorbates are not simply related to their binding energy, as most of the adsorbates are knocked off the surface by collisions with substrate atoms. Thus the energy distribution of the ejecting substrate atoms influences the energy distribution of the adsorbate species. This observation also holds true for the angular distributions, which can be used to give better insight into the ejection mechanisms.

Angular Distributions

The energy-integrated angular distributions of C_6H_6 molecules detected along the $\phi = -30°$ azimuth, which represents the strongest channeling direction for the {111} surface, are shown in Figure 7. Both the calculated angular spectrum and the experimental distribution for low coverage (∼0.05 ML)[46] have a strong off-normal peak close to $\theta \approx 40°$. This structure in the angular distribution indicates that the ejected C_6H_6 molecules reflect the directional character of the ejected substrate metal atoms[47−49] which also have a large peak at $\theta \approx 40°$. There is a slight unexplained discrepancy between the experimental and calculated distributions in that the experimental distribution has a peak in the normal direction ($\theta = 0°$) whereas the calculated distribution peaks at $\theta \approx 10°$. The off-normal peak disappears
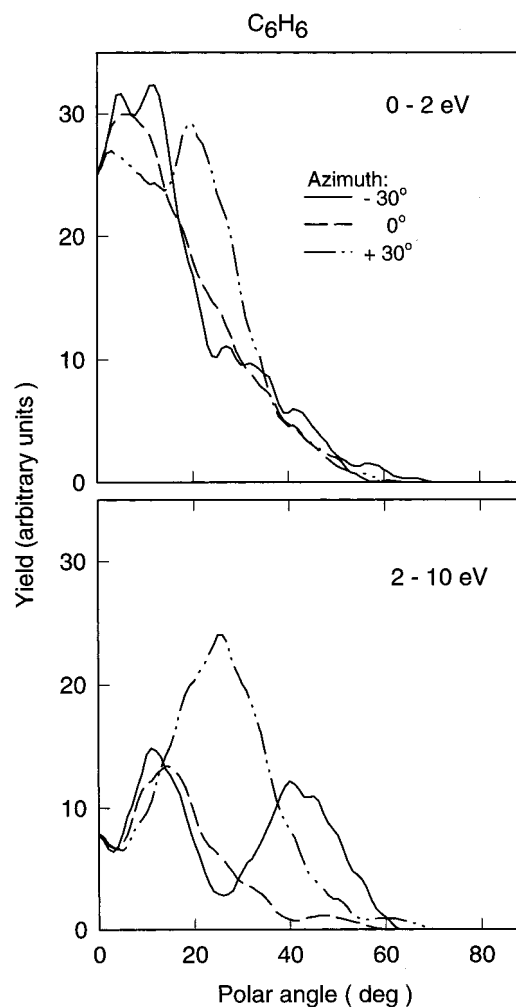
C_6H_6
energy integrated
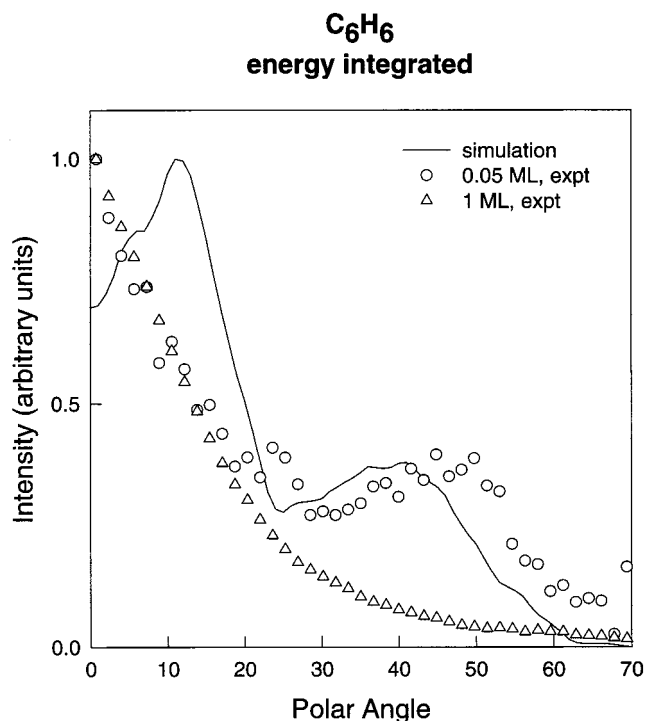
Figure 7. The angular distributions of C_6H_6 obtained from the MD simulation and experiments performed for two different C_6H_6 coverages and for the $\phi = -30°$ azimuth.

when the C_6H_6 coverage is increased to 1 ML in the experiment. The coverage-dependent angular distributions of the atomic adsorbate are discussed later to explain this trend.

The kinetic energy resolved angular distributions of C_6H_6 along the $\phi = -30°$, 0° and +30° azimuths are shown in Figure 8. These distributions show that the ejection at $\theta \approx 10°$ polar angle occurs predominantly at lower kinetic energies (≤ 2 eV) for all the three azimuths and is nearly isotropic. The high-energy (>2 eV) angular distributions exhibit ejection at $\theta \approx 10°$ only along the $\phi = -30°$ and 0° azimuths. The angular distribution along the $\phi = +30°$ azimuth has a single peak at the $\theta \approx 25°$ polar angle. The angular distribution along $\phi = -30°$ azimuth contains both normal and off-normal peaks. The off-normal peak at $\theta \approx 40°$ polar angle is therefore a signature of the high-energy ejection along the $\phi = -30°$ azimuth. Based on these observations, the ejection of C_6H_6 molecules can be placed into three catagories, the off-normal ejection along the $-30°$ azimuth, the off-normal ejection along the $+30°$ azimuth and the normal ejection common to all three azimuths. These mechanisms are discussed in detail in a separate section below.

Also interesting to note is that the peak intensity along $\phi = +30°$ is higher than that along the $\phi = -30°$ azimuth. This behavior is quite different from the atomic ejection from {111} metal surfaces where the off-normal ejection along the $\phi = -30°$ azimuth is dominant.[47] To better explain the observed results, it is again important to determine whether this is an adsorbate (atomic or molecular) effect or whether this is unique only to molecular films.

The angular distributions of the atomic adsorbate are shown in Figure 9 for the (3 × 3) and (1 × 1) ordered overlayers. The distribution for the (3 × 3) overlayer has a strong peak at the $\theta \approx 50°$ polar angle along the $\phi = +30°$ azimuth. No prominent peaks are observed along the $\phi = -30°$ and 0° azimuths. The ejection along $\phi = +30°$ is the strongest, similar for the ejection of C_6H_6 molecules. As mentioned earlier, this does not correspond to the most prominent emission of substrate atoms for

C_6H_6

Figure 8. The calculated energy resolved angular distributions of C_6H_6 molecules with kinetic energies (a) below 2 eV and (b) above 2 eV along the three azimuths.

{111} surfaces which occurs along the $\phi = -30°$ azimuth. Therefore, the ejection characteristics of atomic and molecular adsorbates are different from the ejection from clean surfaces.

The coverage-dependent angular distributions of the atom exhibit trends similar to those observed in the experimental angular distributions of C_6H_6 molecules. The distribution for the (1 × 1) atomic overlayer exhibits only the peak in the normal direction for all the three azimuths (Figure 9), as is the case for C_6H_6 molecule distributions obtained at 1ML coverage (Figure 7). The anisotropy visible in the angular distributions for the lower coverage, (3 × 3) overlayer for the atom and 0.05 ML for the C_6H_6 molecule, is no longer present. The motions are randomized by the increased interparticle collisions at the higher coverage. These observations indicate that the adsorbate angular distributions at high coverage do not exhibit the anisotropic behavior known to be a signature for ordered metal surfaces, regardless of whether the ordered overlayer consists of atoms or molecules.

Ejection Mechanisms

The strength of the MD approach is that insight into microscopic processes that lead to specific features in measured distributions can be extracted. The extremely good match between the calculated and experimental kinetic energy and angular distributions encourages us to proceed with a mechanistic investigation for molecular ejection. The high-energy
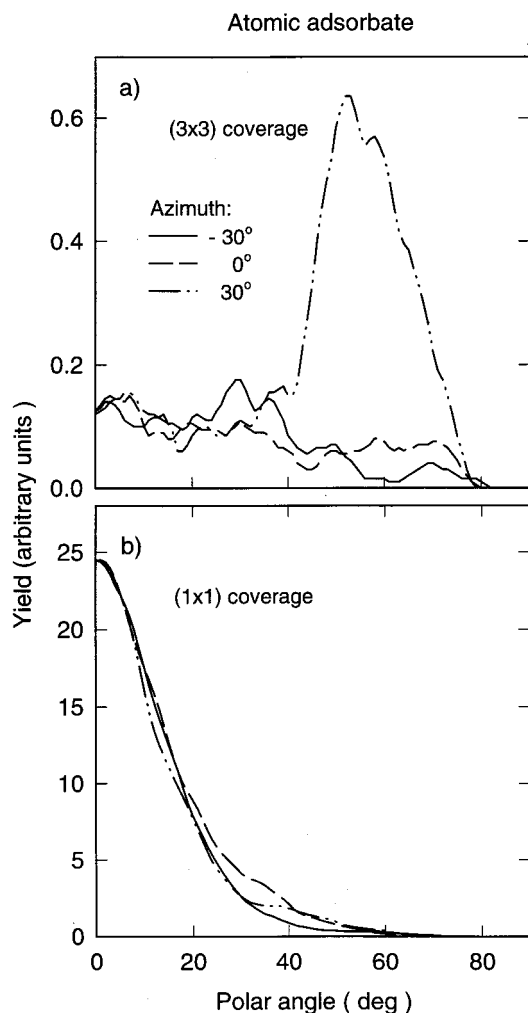
Figure 9. The calculated energy resolved angular distributions of the atomic adsorbate along the three azimuthal directions for (a) (3 × 3) and (b) (1 × 1) coverage.

projectile bombardment initiates a collision cascade in the Ag substrate. Any direct collision between a C_6H_6 molecule and the primary particle is rare and also fragments the molecule immediately, thus, the collision does not contribute to molecular ejection. It is both single and multiple collisions with substrate Ag atoms moving toward the vacuum that initiate the ejection of intact C_6H_6 molecules. Depending on the trajectory, the emitted molecules can be located either far away or close to the impact point of the initial projectile. Benzene ejection due to collisions from one Ag atom is found to be the more energetic. In this case the molecule, which initially lies flat on the surface, tilts from the side as it is hit by a Ag atom until it has sufficient energy to move off from the surface. Multiple collisions by two or more Ag atoms mostly result in ejection at lower kinetic energies. As mentioned earlier, the collision processes leading to intact C_6H_6 molecular ejection can be categorized into three different mechanisms which correlate with their energy and angle of ejection.

The first mechanism, as shown in Figure 10, describes the off-normal ejection along the $\phi = -30°$ azimuth. Benzene molecules eject mainly due to a single collision from an adjacent first-layer atom. As indicated by the arrows in the figure, an energetic first-layer Ag atom (which does not lie below the C_6H_6) moves directly toward the C_6H_6 molecule from one side. In doing so, this energetic atom pushes the two first-layer Ag atoms that are right below the molecule (top view at 100 fs),

and then makes a direct collision with the molecule from the side. This sequence explains why the ejection occurs at an off-normal angle close to $\theta \approx 40°$. The first-layer atom colliding with the C_6H_6 molecule acquires its energy either directly from the projectile or from another first-layer atom. This type of collision occurs only along the $\phi = -30°$ azimuth. For other azimuths the adjacent first-layer atoms would not be able to directly hit the molecule without first hitting another first-layer atom located directly below the molecule.

The second mechanism, as shown in Figure 11, describes the off-normal ejection angle at $\theta \approx 25°$ along the $\phi = +30°$ azimuth. As in the earlier case, the benzene molecules eject mainly due to a single collision with the substrate first-layer atom. This time, however, the first-layer Ag atom is located right below the molecule. This first-layer atom gets its energy either from a second-layer atom or another first-layer atom that was reflected from the second layer. In either case an atom hits the first-layer atom from below. Since the molecules are ejected due to a collision with a Ag atom right below it, the ejection angle is closer to normal ($\sim 25°$) compared to the earlier case. These collisions also tend to be energetic.

The third mechanism, as shown in Figure 12, describes the near-normal ejection along all three azimuths. Benzene molecules eject mainly due to multiple collisions with first-layer Ag atoms located right below the molecule. Since two or more atoms hit the molecule, the initial directionality is lost and the molecules eject in a near-normal direction. Molecules emitted by this mechanism tend to have lower kinetic energies. This type of ejection mainly occurs a long time after the primary particle impact when the collision cascade has had sufficient time to develop in the solid. It is therefore difficult to trace the collisional sequence back to the projectile.

Predictions

The simulation results can also be used to make predictions for future experiments. The correlation of the kinetic energies of the molecules with their internal energies is important from an experimental viewpoint. The calculated internal energy resolved kinetic energy distributions, as shown in Figure 13, can be used to predict how the kinetic energy distributions would behave if a vibrational state selective study of C_6H_6 were performed. The calculations show that the kinetic energy distribution strongly depends on the degree of internal excitation of the C_6H_6 molecules. The kinetic energy distribution of molecules with internal energies between 0 and 0.5 eV is much narrower and peaks at a lower energy than the distribution of molecules with internal energies between 0.5 and 5 eV. Since the vibrational spectrum of C_6H_6 is well studied,[50] it should therefore be possible to design an experiment in which resonant ionization is used to measure the kinetic energy distribution of C_6H_6 molecules within a specific vibrational mode. It would be interesting to monitor experimentally this predicted change in the kinetic energy distribution as a function of the vibrational state of the molecule.

The simulations also show that the ejection of C_6H_6 along the $+30°$ azimuth is higher than that along $-30°$ azimuth. Angular distribution measurements of C_6H_6 at low coverage performed along all three azimuths will be valuable to prove experimentally this calculated result. Also the simulations show that the angular distributions strongly depend on the adsorbate site. As shown in Figure 14, the angular distributions of the atomic adsorbate are very different for the fcc 3-fold site (i.e., above a third-layer atom) versus the hcp 3-fold site (i.e., above a second-layer atom). Benzene is known to adsorb on different

Off-normal Ejection along -30° Azimuth

Top view

t=0 fs   t=100 fs

Side view
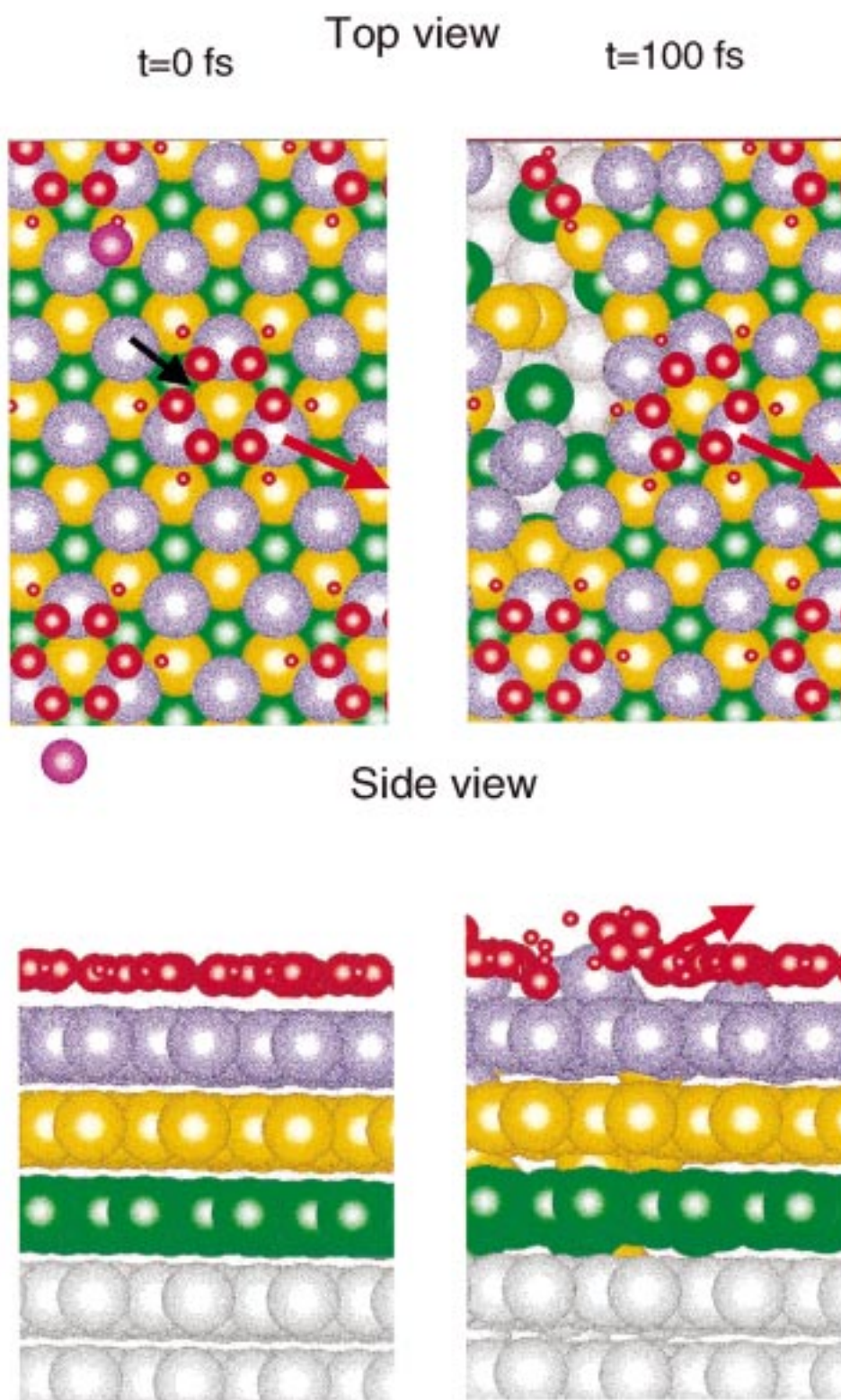
Figure 10. A mechanistic view of the off-normal ejection along the $\phi = -30°$ azimuth. The black arrows represent the collisions in the solid and the red arrow shows the direction in which the molecule ejects. This color pattern is repeated in Figures 11 and 12.

sites depending on the metal surface.[51] Angular distribution measurements of C$_6$H$_6$ adsorbed on different sites of a {111} surface would show how the distributions change with the adsorbate site.

Conclusion

Molecular dynamics calculations of keV particle bombardment of a (3 × 3) ordered overlayer of C$_6$H$_6$ on Ag{111} have

# Off-normal Ejection along +30° Azimuth

Top view
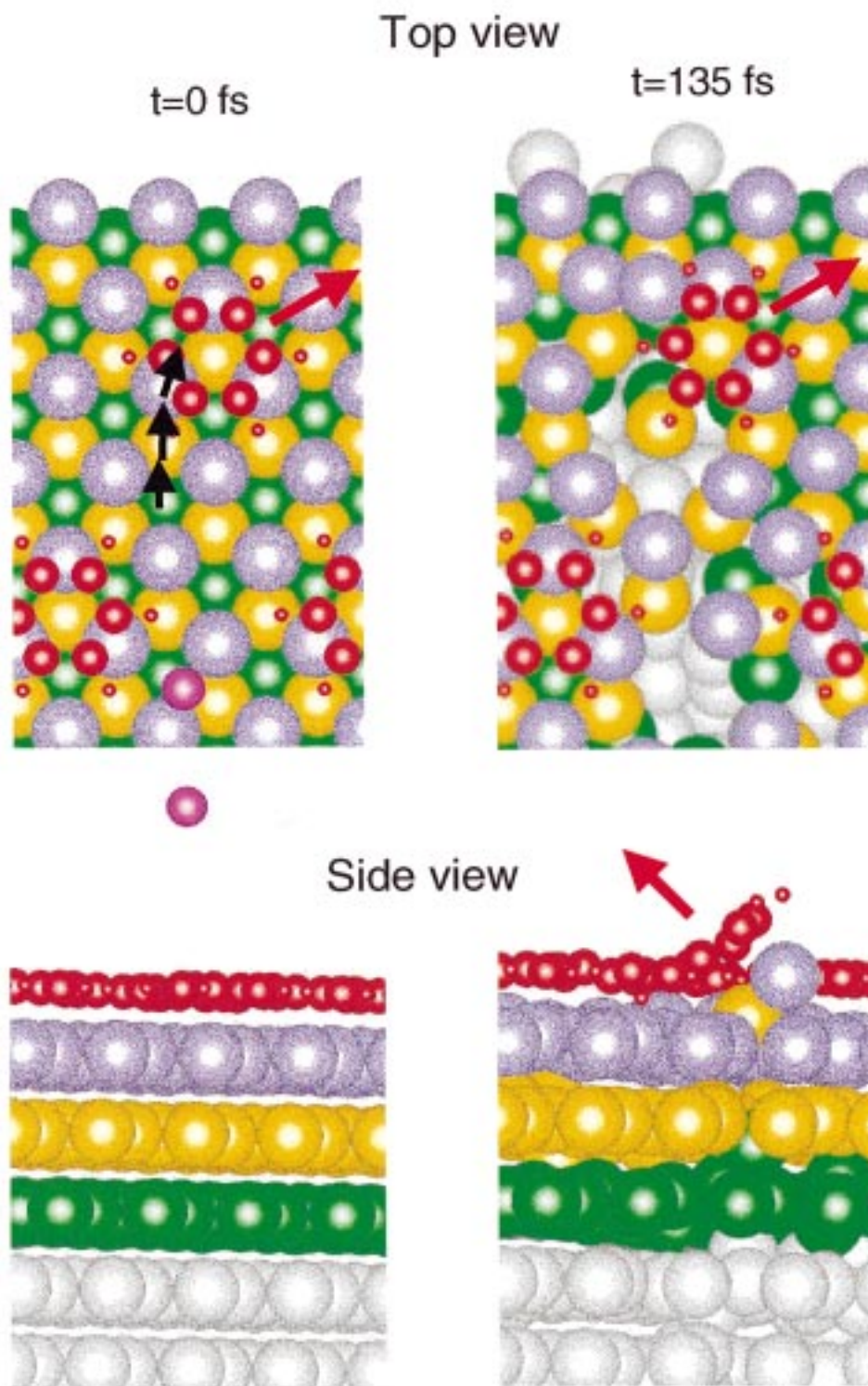
Figure 11. A mechanistic view of the off-normal ejection along the $\phi = +30°$ azimuth.

been performed. The calculated kinetic energy and angular distributions of neutral C_6H_6 molecules are compared with experimental data measured after keV Ar^+ ion bombardment of thin films of C_6H_6 on Ag{111} using nonresonant multiphoton ionization. The calculated spectra reproduce the experimental observations very well. The angular distributions of C_6H_6 indicate the occurrence of a strong off-normal ejection along with the predominant normal ejection. This anisotropy indicates that C_6H_6 molecules retain some of the directional character associated with the collision cascade in the metal. The off-normal peak in the angular distribution, however, disappears as the C_6H_6 coverage is increased. The angular distributions of

Normal Ejection along all Azimuths

Top view

t=0 fs

t=135 fs

Side view
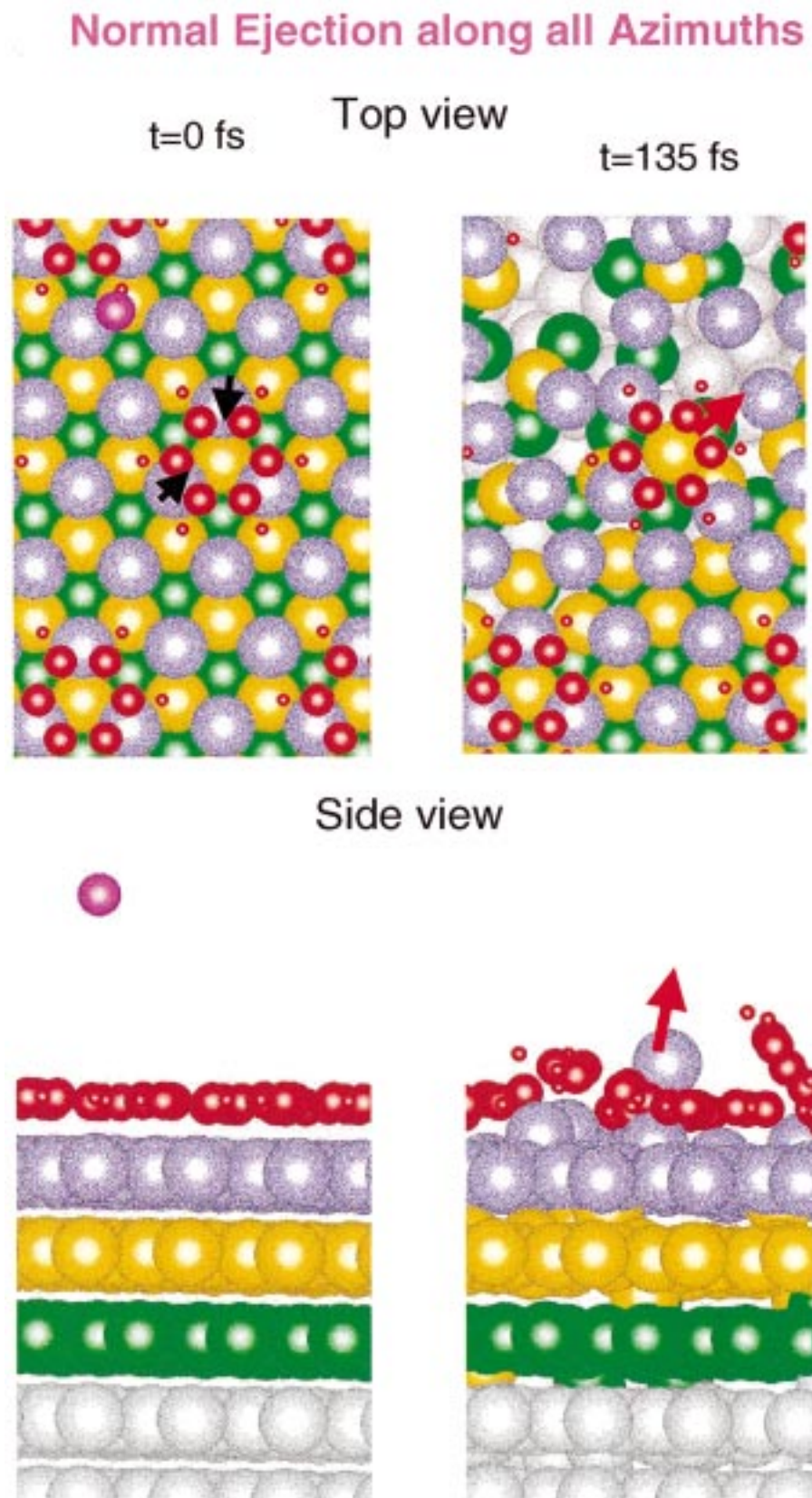
Figure 12. A mechanistic view of the normal ejection.

an adsorbate at high coverage do not exhibit the anisotropic behavior observed in ordered metal surfaces, regardless of whether the ordered overlayer consists of atoms or molecules.

Simulations show that coverage has a strong influence on the kinetic energy distributions of the adsorbate. This trend is also observed in the experimental kinetic energy distributions of C_6H_6 as a function of coverage. An increase in the overlayer coverage increases interparticle collisions, thereby reducing the peak kinetic energy of the overlayer atom or molecule. The energy distributions are also influenced by the energy distribution of substrate metal atoms.

Mechanistic investigations show that intact C_6H_6 molecules
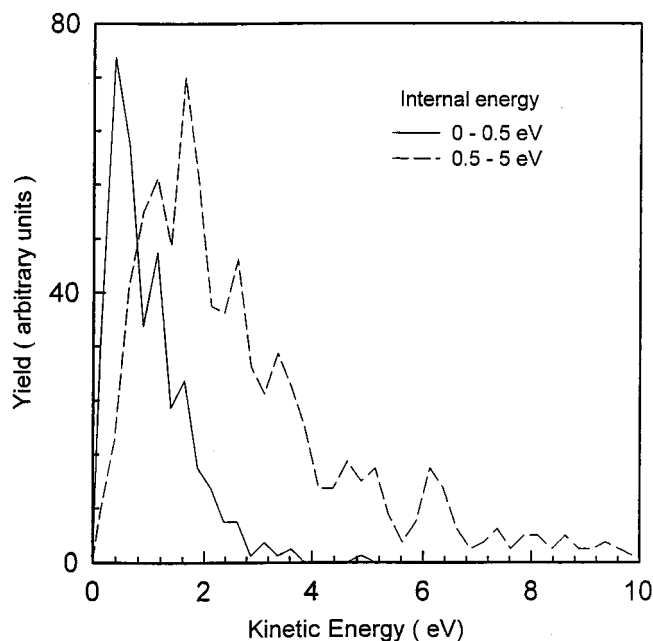
Figure 13. The calculated internal energy resolved kinetic energy distributions of C_6H_6 molecules.
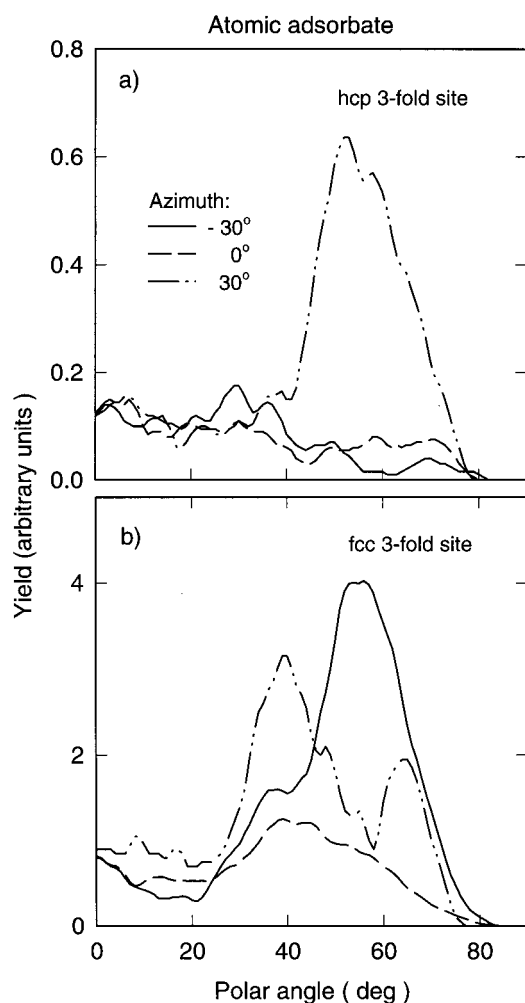
Figure 14. The calculated energy resolved angular distributions of the atomic adsorbate as a function of adsorbate site along the three azimuthal directions.

located both far away and close to the impact point are ejected. The C_6H_6 molecules that are directly hit by the projectile fragment immediately. Both single and multiple collisions from the substrate Ag atoms lead to ejection of C_6H_6 molecules. Ejection due to single collisions is found to be more energetic while those due to multiple collision result in low-energy ejection. In general, off-normal ejection is stimulated by single collisions while emission of molecules in directions close to the surface normal is stimulated by multiple collisions. The collision process leading to C_6H_6 ejection can be categorized into three different mechanisms based on the polar ejection angle and the azimuth direction. First, the off-normal ejection along the $-30°$ azimuth occurs mainly due to single collision from a first-layer atom initially located at the side of the molecule. Second, the off-normal ejection along the $+30°$ azimuth occurs predominantly due to single collision with a first-layer atom initially located right below the molecule. Third, the normal ejection along all the three azimuths occurs mainly due to multiple collisions from first-layer atoms initially located below the molecule.

Finally, we have used the simulation results to predict how the kinetic energy distributions would behave if a vibrational state selective study of C_6H_6 were performed. The calculations show that the kinetic energy distribution peaks at a lower value and is much narrower for molecules with low internal energies as compared to those with high internal energies. It is possible to design an experiment to measure this predicted change in the kinetic energy distribution as a function of the vibrational state of the C_6H_6 molecule.

References and Notes

(1) Permanent address: Institute of Physics, Jagellonian University, ul. Reymonta 4, PL-30059, Krakow 16, Poland.

(2) Secondary Ion Mass Spectrometry SIMS XI; Gillen, G., Lareau, R., Bennett, J., Stevie, F., Eds.; John Wiley & Sons: New York, 1998.

(3) Chatterjee, R.; Riederer, D. E.; Postawa, Z.; Winograd, N. *J. Phys. Chem.* **1998**, *102*, 4176.

(4) Chatterjee, R.; Riederer, D. E.; Postawa, Z.; Winograd, N. *Rapid Comm. in Mass Spectrom.* **1998**, *12*, 1226.

(5) Urbassek, H. M. *Nucl. Instrum. Methods Phys. Res.* **1987**, *B18*, 587.

(6) Haring, R. A.; Roosendaal, H. E.; Zalm, P. C. *Nucl. Instrum. Methods Phys. Res.* **1987**, *B28*, 205.

(7) Hoogerbrugge, R.; Kistemaker, P. G. *Nucl. Instrum. Methods Phys. Res.* **1987**, *B18*, 600.

(8) Haring, R. A.; Pedrys, R.; Oostra, D. J.; de Vries, A. E. *Nucl. Instrum. Methods Phys. Res.* **1984**, *B5*, 483.

(9) Urbassek, H. M.; Michl, J. *Nucl. Instrum. Methods Phys. Res.* **1987**, *B22*, 400.

(10) Kelly, R. *Nucl. Instrum. Methods Phys. Res.* **1990**, *B46*, 441.

(11) Riederer, D. E.; Chatterjee, R.; Rosencrance, S. W.; Postawa, Z.; Dunbar, T. D.; Allara, D. L.; Winograd, N. *J. Am. Chem. Soc.* **1997**, *119*, 8089.

(12) Pedrys, R.; Oostra, R. A.; Haring, A.; Calcagno, L.; Haring, A.; de Vries, A. E. *Nucl. Instrum. Methods Phys. Res.* **1986**, *B17*, 15.

(13) Haring, R. A.; Pedrys, R.; Oostra, D. J.; Haring, A.; de Vries, A. E. *Nucl. Instrum. Methods Phys. Res.* **1984**, *B5*, 476.

(14) Chatterjee, R.; Riederer, D. E.; Postawa, Z.; Winograd, N. Unpublished results.

(15) Harrison, D. E., Jr. *CRC Crit. Rev. Solid State Mater. Sci.* **1988**, *14*, S1.

(16) Garrison, B. J.; Winograd, N.; Lo, D.; Tombrello, T. A.; Shapiro, M. H.; Harrison, Jr., D. E. *Surf. Sci. Lett.* **1987**, *180*, L129.

(17) Bernardo, D. N.; Bhatia, R.; Garrison, B. J. *Comput. Phys. Comm.* **1994**, *80*, 259.

(18) Rosencrance, S. W.; Burnham, J. S.; Sanders, D. E.; He, C.; Garrison, B. J.; Winograd, N.; Postawa, Z.; DePristo, A. E. *Phys. Rev. B* **1995**, *52*, 6006.

(19) He, C.; Rosencrance, S.; Postawa, Z.; Xu, C.; Chatterjee, R.; Reiderer, D. E.; Garrison, B. J.; Winograd, N. *Nucl. Inst. Methods B* **1995**, *100*, 209.

(20) King, B. V.; Zimmerman, C.; Riederer, D. E.; Rosencrance, S. W.; Garrison, B. J.; Winograd, N. *Rapid Comm. in Mass Spectrom.* **1998**, *12*, 1236.

(21) Garrison, B. J. *J. Am. Chem. Soc.* **1980**, *102*, 6553.

(22) Garrison, B. J. *J. Am. Chem. Soc.* **1982**, *104*, 6211.

(23) Garrison, B. J. *Int. J. Mass Spectrom. Ion Phys.* **1983**, *53*, 243.

(24) Brenner, D. W. *Phys. Rev. B* **1990**, *42*, 9458.

(25) Brenner, D. W.; Harrison, C. T.; White, C. T.; Colton, R. J. *Thin Solid Films* **1991**, *206*, 220.

(26) Taylor, R. S.; Garrison, B. J. *Langmuir* **1995**, *11*, 1220.

(27) Taylor, R. S.; Garrison, B. J. *Int. J. Mass. Spectrom. Ion Processes* **1995**, *143*, 225.

(28) Taylor, R. S.; Garrison, B. J. *Chem. Phys. Lett.* **1994**, *230*, 495.

(29) Taylor, R. S.; Brummel, C. L.; Winograd, N.; Garrison, B. J.; Vickerman, J. C. *Chem. Phys. Lett.* **1995**, *233*, 575.

(30) Taylor, R. S.; Garrison, B. J. *J. Am. Chem. Soc.* **1994**, *116*, 4465.

(31) Liu, K. S. S.; Vickerman, J. C.; Garrison, B. J. *Radiat. Eff. Defects Solids* **1997**, *142*, 205.

(32) Zaric, R.; Pearson, B.; Krantzman, K.; Garrison, B. J. *Int. J. Mass Spectrom. Ion Processes* **1998**, *174*, 155.

(33) Garrison, B. J. *Chem. Soc. Rev.* **1992**, *21*, 155.

(34) Garrison, B. J.; Winograd, N.; Harrison, D. E., Jr. *J. Chem. Phys.* **1978**, *69*, 1440.

(35) Dudde, R.; Frank, K. H.; Koch, E. E. *Surf. Sci.* **1990**, *225*, 267.

(36) Stave, M. S.; Sanders, D. E.; Raeker, T. J.; DePristo, A. E. *J. Chem. Phys.* **1990**, *93*, 4413.

(37) Raeker, T. J.; DePristo, A. E. *Int. Rev. Phys. Chem.* **1991**, *10,* 1.

(38) Kelchner, C. L.; Halstead, D. M.; Perkins, L. S.; Wallace, N. M.; DePristo, A. E. *Surf. Sci.* **1994**, *310*, 425.

(39) O'Connor, D. J.; MacDonald, R. J. *Radiation Effects* **1977**, 34, 247. For all Ar interactions and the zirconium−zirconium interactions, we used the Firsov screening length. For the Ag−C and Ag−H interactions we used eq 6 of this reference in order to obtain a better spline fit to the Lennard−Jones potential.

(40) Garrison, B. J.; Kodali, P. B. S.; Srivastava, D. *Chem. Rev.* **1996**, *96*, 1327.

(41) The binding energy of C_6H_6 on Cu{111} is 0.6 eV. Since Ag is less reactive than Cu, the binding energy in this case should be lower. A value of 0.4 eV should be a reasonable one.

(42) Anderson, A. B.; McDevitt, M. R.; Urbach, F. L. *Surf. Sci.* **1984**, *146*, 80.

(43) Liu, K. S. S.; Yong, C. Y.; Garrison, B. J.; Vickerman, J. C. Unpublished results.

(44) Wucher, A.; Garrison, B. J. *Phys. Rev. B.* **1992**, *46*, 4855.

(45) Thompson, M. W. *Philos. Mag.* **1968**, *18*, 377.

(46) Whereas the kinetic energy distributions are identical for coverages less than 0.2 ML, the angular distributions do exhibit a coverage dependence in the very low coverage regime (Ref. 3). Thus we chose 0.2 ML for the kinetic energy distribution plots as the signal-to-noise ratio is greater and 0.05 ML for the angular distributions as they are the lowest coverage ones available.

(47) Holland, S. P.; Garrison, B. J.; Winograd, N. *Phys. Rev. Lett.* **1979**, *43,* 220.

(48) Holland, S. P.; Garrison, B. J.; Winograd, N. *Phys. Rev. Lett.* **1980**, *44*, 756.

(49) Garrison, B. J.; Winograd, N.; Deaven, D. M.; Reimann, C. T.; Lo, D. Y.; Tombrello, T. A.; Harrison, D. E., Jr.; Shapiro, M. H. *Phys. Rev. B.* **1988**, *37*, 7197.

(50) Callomon, J. H.; Dunn, T. M.; Millis, I. M. *Philos. Trans. A.* **1966**, *259*, 499.

(51) Somorjai, G. A. *Introduction to Surface Chemistry*; John Wiley & Sons: New York, and 1994; references therein.